CRYSTAL GROWTH & DESIGN

pubs.acs.org/crystal

Article

Selective Loading of Xylene Isomers in Self-Assembled Triphenylamine *bis*-Urea Macrocycles

Dustin W. Goodlett, Ammon J. Sindt, Md Faizul Islam, Mark D. Smith, and Linda S. Shimizu*

Cite This: *Cryst. Growth Des.* 2022, 22, 1017−1023

Read Online

ACCESS | Metrics & More | Article Recommendations | Supporting Information

ABSTRACT: Supramolecular self-assembly of brominated triphenyl amine *bis*-urea macrocycles leads to the formation of porous organic crystals with small elliptical 4.3 Å × 6.5 Å unidirectional pores. Here, this porous material has been applied in a simple vapor loading technique for the enrichment of isomeric mixtures of xylene. The host exhibits selectivity toward loading linear isomers present in the mixture that better match the channel topography. The same crystals were reused for multiple separations, highlighting the robust nature of the crystals. Host−guest complexes with each xylene constitutional isomer as well as with ethylbenzene were separately prepared by single-crystal-to-single-crystal guest exchange and their structures analyzed by single-crystal X-ray diffraction. Room-temperature xylene isomer enrichment employing these porous organic crystals provides insight toward energy efficient alternatives for separating complex petrochemical feed mixtures.

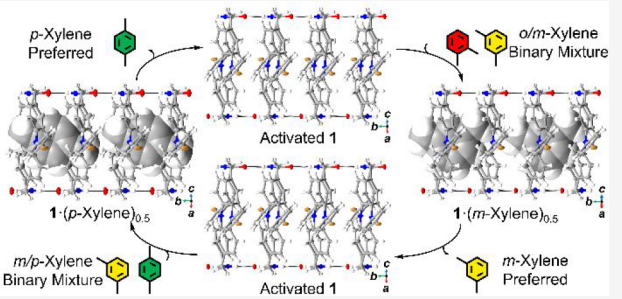

Porous materials serve as vessels for small molecules and are useful for storage, sensing, and separations.[1−8] For example, the separation of C8 aromatic compounds (xylene isomers and ethylbenzene (EB)) found in crude oil is important for commercial materials but is a challenging process with a high energy cost.[9] Xylene isomers have similar physiochemical properties including boiling points and vapor pressures and are not easily separated by distillation.[9−11] Melt crystallization is hindered by the eutectic point, limiting isomer enrichment to 70%.[9] Currently, adsorption purification, considered to be energy-friendly, accounts for ∼75% of the xylene enrichment processes worldwide.[9] These processes typically employ zeolites, which have low manufacturing costs, MOFs, or organic porous materials.[12−24] Adsorption purification has also been achieved using nonporous materials such as Werner clathrates,[25] switchable coordination networks,[26] and molecular hosts.[27] Some of these materials are impacted by water in the feed mixtures or exhibit stability issues in the presence of water or acidic solutions.[7,9,28] Here, we apply a porous crystalline host from self-assembled triphenylamine *bis*-urea macrocycle **1** depicted in Figure 1 to separate stocks of ortho, meta, and para xylenes (*o*-X, *m*-X, *p*-X). To simulate how host **1** could be used for the separation of C8 aromatic compounds from crude oil, EB was loaded into the porous channels of **1** and competition experiments with mixtures of the four compounds were also investigated. Interestingly, the kinetic diameters of these guests range from 6.7 to 7.4 Å (Table 1), similar to the pore size of host **1**.[29] In addition, the single crystal structures of the host−guest complexes were obtained and compared (Figure 2A).

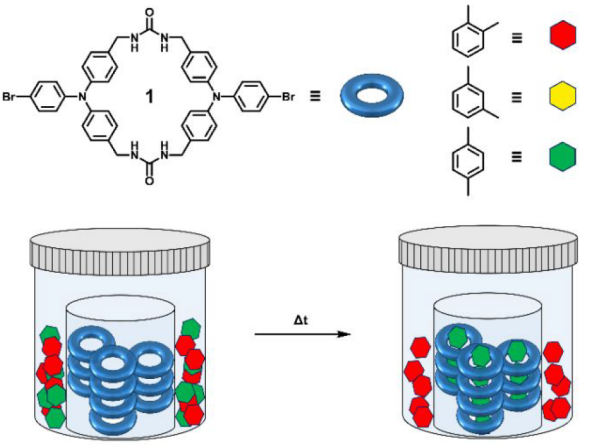

Figure 1. Self-assembly of **1** into porous tubes used for enrichment of binary xylene isomeric mixtures via vapor loading at room temperature. *p*-X (green) is most favored to load into activated host **1**.

Host **1** is an example of a bottom-up assembly approach and relies on a macrocyclic building block with an inherent internal pore to reliably form pores upon assembly and crystalliza-

Received: July 26, 2021
Revised: December 12, 2021
Published: December 30, 2021

https://doi.org/10.1021/acs.cgd.1c00846
Cryst. Growth Des. 2022, 22, 1017−1023

Table 1. Physical Properties of C8 Aromatic Compounds[10,29,30]

isomer	boiling point (K)	kinetic diameter (Å)	dipole moment ($\times 10^{18}$ esu cm)	polarizability ($\times 10^{-25}$ cm^3)
o-X	417.6	7.4	0.649	141−149
m-X	412.3	7.1	0.36	142
p-X	411.5	6.7	0.1	137−149
EB	409.3	6.7	0.59	142

tion.[31,32] The three centered urea−urea hydrogen bonding motif (Figure 2B) guides the construction of columns while the exterior bromines contribute additional halogen-π contacts to facilitate the packing of the one-dimensional columns.[33] The multiple and directional intermolecular contacts of **1** enhance production of larger crystals (35 × 265 μm), which are robust enough to load guests via single-crystal-to-single-crystal (SC−SC) transformations.[34] Crystals are activated by simple heating to remove the encapsulated solvent of crystallization and afford host **1**. Exposure of host **1** to new guests in the liquid or vapor phase results in uptake of the guest to give crystals of a new host−guest complex, which readily diffract by SC-XRD. The elliptical 4.3 Å × 6.5 Å unidirectional pores of assembled **1** (Figure 2A) readily load small planar guests including benzene and its halogenated derivatives.[34] All host−guest complexes observed with SC-XRD retained the hydrogen bonding network of the host after each new guest was exchanged inside.

Here, we investigate if the xylene isomers (*o*-X, *m*-X, *p*-X) can be individually loaded in the channels of **1** and examine the structures and contacts of these host−guest complexes. The xylene isomers with smaller kinetic diameters exhibited favorable geometries for $\pi-\pi$ stacking interactions with the host framework. The host was then tested for the separation of mixed solutions of *o*-X, *m*-X, and *p*-X. Selectivity of guest loading was found to favor the smaller isomer in all competition experiments.

RESULTS AND DISCUSSION

Macrocycle **1** was synthesized as previously reported.[34] Host **1** crystals were grown via vapor diffusion of 1,2-dimethoxyethane (DME) into a dimethyl sulfoxide (DMSO) solution of **1** (~2.5 mg/mL).[34] The crystals (5 mg samples) were activated by heating to 80 °C under vacuum overnight, then cooled under vacuum to room temperature. Next, vials of activated host **1** were removed from vacuum and placed inside larger vials containing prepared binary xylene mixtures for competition experiments or in pure xylene samples for SC−SC transformation studies (Figure 1). In all cases, xylene guests were allowed to vapor load into the activated host **1** crystals overnight and crystals remained colorless throughout the 54 competition studies and four single component sorption experiments using the same batch of crystals. Additionally, a competition experiment was conducted on a ternary xylene mixture as well as a quaternary mixture including the three xylene isomers and ethylbenzene (Figure 5A,B). The guests were subsequently extracted from the complexes using CH_2Cl_2.

To assess if the C8 aromatics can be absorbed individually into the host, we first characterized the complexes by SC-XRD. Table S1 compares the single crystal SC-XRD data for the activated host **1** (CCDC No. 1899528) with **1**·(*o*-X)$_{0.5}$ (CCDC No. 2097958), **1**·(*m*-X)$_{0.5}$ (CCDC No. 2097959),

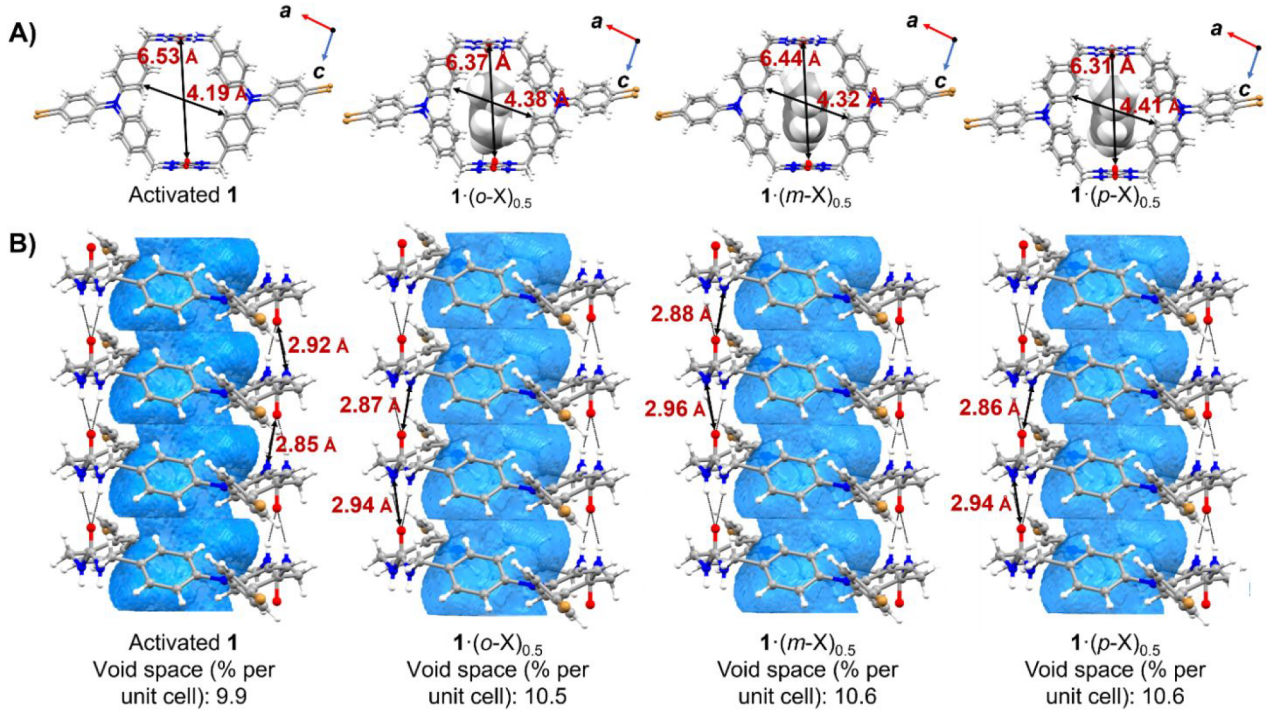

Figure 2. (A) Comparison of interatomic distances within the pores of activated **1**, **1**·*o*-X, **1**·*m*-X, and **1**·*p*-X as viewed along the crystallographic *b*-axis from SC-XRD data (subtracting for van der Waals radii). (B) Comparison of one-dimensional columns of activated host **1**, **1**·*o*-X, **1**·*m*-X, and **1**·*p*-X with their void space highlighted in blue and urea−urea hydrogen bond distances labeled. Xylene guests were removed for all void space calculations. Columnar void space was calculated with a probe radius of 1.3 Å and approximate grid spacing of 0.1 Å using the Mercury 2020.2.0 software package.[35]

https://doi.org/10.1021/acs.cgd.1c00846
Cryst. Growth Des. 2022, 22, 1017−1023

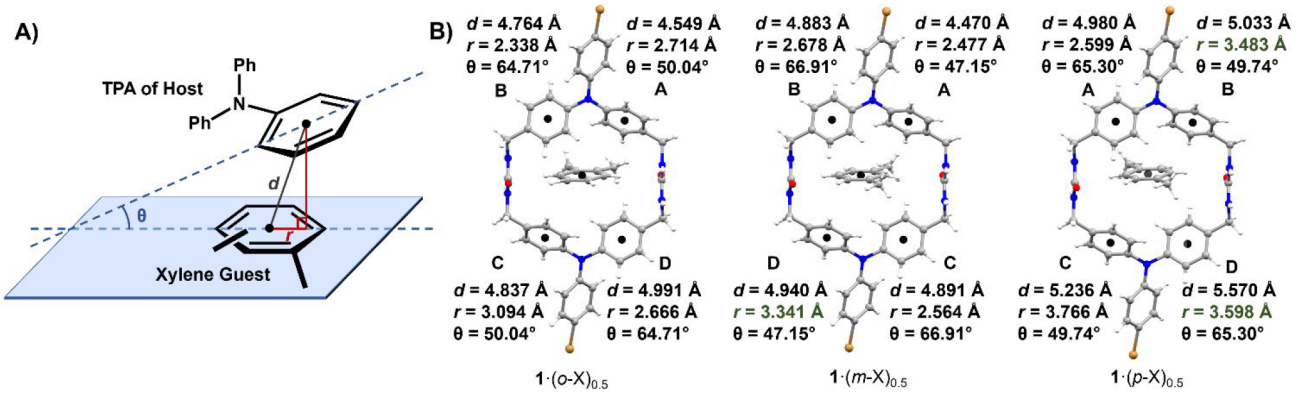

Figure 3. (A) Schematic diagram illustrating key attributes for $\pi-\pi$ interactions: centroid−centroid distance (d), centroid−centroid offset (r), and interplanar angle (θ). (B) The xylene guest and nearest macrocycle from each of the complexes. Key attributes for $\pi-\pi$ interactions are listed beside the aryl rings making up the inner pore of host **1**. The aryl rings are labeled A−D in order by increasing centroid−centroid (d) distance between the host and guest. Offset values (r) that fall within the most commonly reported range are highlighted in green.[36]

1·(p-X)$_{0.5}$ (CCDC No. 2097960), **1**·(EB)$_{0.45}$ (CCDC No. 2121650), and **1**·(CH_2Cl_2)$_{0.52(1)}$ (CCDC No. 2097957). The activated host crystals and its clathrates adopt the $P2_1/c$ space group of the monoclinic system. In each case, no dissolution or change in crystal size was observed throughout the process, consistent with guest loading via a nondestructive SC-SC transformation. The xylene isomers each displayed 1:0.5 host−guest stoichiometry in their respective complexes.

The pore size of individual macrocycles in the activated host and each host−guest complex varied only very slightly, presumably to better accommodate interactions with each specific guest shape (Figure 2A). The pore of activated **1** exhibits the largest distance (6.53 Å) between the two urea moieties of the assembled macrocycles but the shortest distance (4.19 Å) between the triphenylamine (TPA) spacers.[34] Columnar assembly of macrocyclic **1** expands this inherent cavity to create a porous roughly tubular channel, which oscillates between slightly wider and more narrow sections (Figure 2B). The urea−urea hydrogen bond distances of activated **1** display N(H)···O distances of 2.845(2) and 2.915(2) Å.[34] The void space within these tubes is calculated with Mercury using the single crystal data and reveals the void space of activated **1** to comprise 9.9% of the unit cell.[34]

Figure 2B compares the view along a single column of each xylene complex, highlighting the similar columnar framework of the assembled host.[34] Slight changes were observed upon guest loading. Adsorption of o-X, the largest guest (kinetic diameter = 7.4 Å),[29] affords a **1**·(o-X)$_{0.5}$ complex that exhibits a slight lengthening of the tubes with N(H)···O distances of 2.871(4) and 2.942(4) Å (Figure 2B). The elliptical shaped pores display intermediate urea−urea (6.37 Å) and TPA-TPA (4.38 Å) distances (Figure 2A) and comprise a calculated void space of 10.5% of the unit cell with the guest omitted. Although o-X guest is disordered in **1**·(o-X)$_{0.5}$ (Figure S3), further analysis suggests CH-π and $\pi-\pi$ interactions between the host and guest aryl rings (Figure 3B). The energy of $\pi-\pi$ interaction depends upon interplanar angle (θ) between the two aryl rings as well as the offset distance (r) between their centroids (Figure 3A).[36] A comprehensive survey of $\pi-\pi$ interactions between aryl rings using 28 177 entries from the CCDC (version 5.39) with centroid-to-centroid distances (d = 0−7 Å), interplanar angles (θ = 0−90°), and offset distances (r = 0−3.6 Å) suggests that a parallel displaced geometry with an offset distance of r = 3.2−3.6 Å is the most common geometry for these interactions.[36] The observed interplanar angles (50.04−64.71°, Figure 3B) between o-xylene and the four aryl rings comprising the pore of the nearest host **1** macrocycle suggest more T-shaped stacking character than parallel displaced. However, the **1**·(o-X)$_{0.5}$ complex does not exhibit favorable offset values for either T-shaped (r = 0°) or parallel displaced (r = 3.2−3.6°) geometries (Figure 3B).[36]

For **1**·(m-X)$_{0.5}$, the bent structure of m-X with a slightly smaller kinetic diameter of 7.1 Å, shows an increase in the N(H)···O distances of the framework (2.880(5) and 2.961(5) Å) (Figure 2B). The urea−urea repeat distance in **1**·(m-X)$_{0.5}$ is therefore the largest in the series of complexes at 4.66 Å. An intermediate TPA−TPA distance of 4.32 Å was observed (Figure 2A). The void space of the porous host in the **1**·(m-X)$_{0.5}$ complex equates to 10.6% of the unit cell. Similar to o-X, this guest was examined for parallel displaced $\pi-\pi$ interactions with the interior aryl rings of the host. Intriguingly, $\pi-\pi$ interactions with one of the host's aryl rings does exhibit an offset value (r = 3.341 Å) within the reported ideal range for parallel displaced geometry (r = 3.2−3.6 Å).[36] However, the interplanar angle (θ = 47.15°) is quite large for the two aryl rings to be considered parallel and none of the offset values are near the ideal (r = 0°) value for a T-shaped geometry.

Absorption of the elongated p-X with the smallest kinetic diameter (6.7 Å, Table 1) affords **1**·(p-X)$_{0.5}$ complex with slightly shorter N(H)···O distances (2.863(5) and 2.939(5) Å). The framework's hydrogen bonding distances are closest to those observed in the activated structure (Figure 2B). The pore displays the shortest urea−urea distance of 6.31 Å and shows a lengthening of TPA−TPA distance to 4.41Å (Figure 2A). The void space of **1**·(p-X)$_{0.5}$ is the same as that of **1**·(m-X)$_{0.5}$ equating to 10.6% of the unit cell (Figure 2B). Geometric analysis for $\pi-\pi$ interactions within the host−guest complex reveals two offset distances (r = 3.483 and r = 3.598 Å) within the reported ideal range for parallel displaced geometry.[36] However, the interplanar angles (θ = 49.74 and 65.30°) between these aryl rings suggest they are not parallel and none of the offset values are near the ideal (r = 0°) value for a T-shaped geometry.

Loading of ethylbenzene yielded structure **1**·(EB)$_{0.45}$ (Figure 5C), which is very similar to the xylene complexes. The columnar structure is best viewed along the crystallographic b-axis (Figures S6 and S7) with a urea−urea distance of 6.37 Å and a TPA−TPA distance of 4.36 Å. The void space in the

https://doi.org/10.1021/acs.cgd.1c00846
Cryst. Growth Des. 2022, 22, 1017−1023

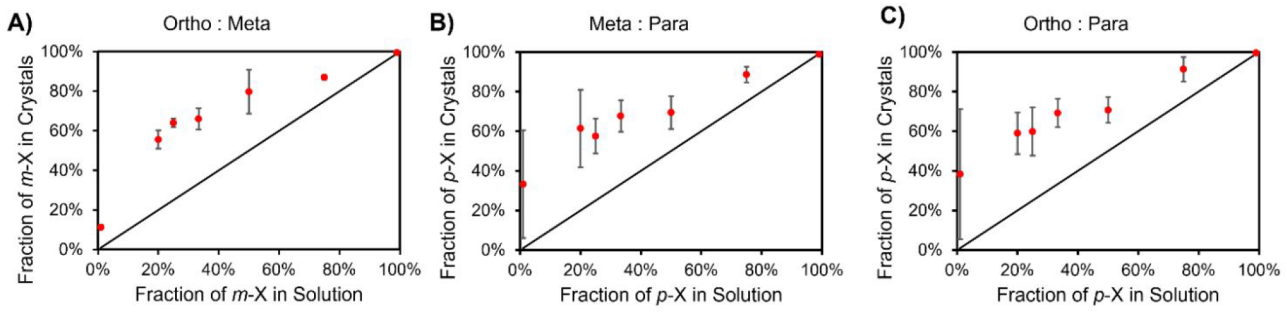

Figure 4. Averaged results from GC/MS data of three trials of selective vapor loading from (A) *o*/*m*-xylene binary mixtures, (B) *o*/*p*-xylene binary mixtures, and (C) *m*/*p*-xylene binary mixture.

channels of the host in **1**·$(EB)_{0.45}$ is 10.4% of the unit cell (Figure S7B). **1**·$(EB)_{0.45}$ exhibits one offset value (r = 3.448 Å, Figure S7C) within the ideal range for parallel displaced $\pi-\pi$ interactions. However, the metrics for the interaction distances in the host−guest complexes are obscured due to the disorder of the guests.

To compare relative strengths of the host−guest interactions for each complex, thermogravimetric analysis (TGA) was conducted on **1**·$(o\text{-X})_{0.5}$, **1**·$(m\text{-X})_{0.5}$, **1**·$(p\text{-X})_{0.5}$, and **1**·$(EB)_{0.45}$ (Figures S8−S12). Each complex exhibited a one-step desorption curve. In **1**·$(p\text{-X})_{0.5}$ the desorption was observed between 25 to 150 °C with an average weight loss of 6.19% (Figure S8), which corresponds to a host/guest ratio of 1:0.51. In comparison, all of the other complexes were slightly less stable, exhibiting a one-step desorption between 25 to 150 °C. **1**·$(o\text{-X})_{0.5}$ exhibited an average weight loss of 5.54%. From the weight loss, we calculated a host/guest ratio of 1:0.45. The **1**·$(m\text{-X})_{0.5}$ showed a weight loss of 5.77% which leads to host/guest ratio of 1:0.47. Finally, **1**·$(EB)_{0.45}$ showed an average weight loss of 5.25% and a host/guest ratio of 1:0.43. Figure S13 compares the desorption curves of the four complexes on one graph and suggests that **1**·$(p\text{-X})_{0.5}$ is slightly more stable than the other three complexes. Another comparison of this stability is the temperature required for 3% weight loss, which was 63, 69, 78, or 96 °C for the **1**·$(m\text{-X})_{0.5}$, **1**·$(EB)_{0.45}$, **1**·$(o\text{-X})_{0.5}$, and **1**·$(p\text{-X})_{0.5}$ complexes, respectively.

To probe selective loading of xylene isomers, binary xylene mixtures were prepared (4 mL each) at the following concentrations using volumetric syringes: 1.00%, 20.0%, 25.0%, 33.3%, 50.0%, 75.0%, and 99.0%. Freshly activated host crystals (5 mg) were exposed to the binary xylene mixtures in a closed container at ambient temp for 16 h (Figure 1). The crystals were then removed from the xylene atmosphere and suspended in CH_2Cl_2 or CD_2Cl_2 for 2 days to ensure complete removal of xylene from the host and replacement with the more favorable CH_2Cl_2 guest. The CH_2Cl_2 guest was then removed under vacuum and the activated hosts were used again to complete three trials of the separation experiment. Samples of the complexes were also directly disassembled by dissolution into DMSO to ensure that extraction does not alter selectivity (Figures S96−S98). We have also used different batches of crystals which quantitively yielded the similar separation of the isomers (Figure S78−S80). Xylene isomers have very similar boiling points and vapor pressures and the vapor loading procedure is not expected to influence the loading selectivity.[10,11]

The extracted solutions were analyzed directly with gas chromatography/mass spectrometry (GC/MS) and ^{1}H NMR (Figures S13−S98). Relative peak intensities from the GC/MS data (Figures S13−S84) were used to determine the relative ratios of each xylene isomer that were loaded inside host **1**. Each experiment was repeated three times to assess the reproducibility of these results, and the standard deviation between the trials at each isomeric ratio are reported in Figure 4A−C and in Table S2.

For the *m*-X versus *o*-X separation, the average percentage of *m*-X adsorbed by host **1** is plotted against the percentage of *m*-X from the prepared solution in Figure 4A. The solid black line in the graph represents zero selectivity. Clearly, measurements of host **1** separation efficiencies are significantly above this threshold indicating selective loading. The data are also tabulated in Table S2. The percentage of *m*-X measured inside host **1** is more than double that of *m*-X from the less concentrated (20.0% and 25.0% *m*-xylene) prepared solutions. Further enrichment of *m*-X solutions at higher concentrations is observed. The 50.0% *m*-X solution lead to an average loading of 79.7 ± 11% *m*-xylene inside the host giving a meta/ortho selectivity value of 3.9 which is comparable to that of a Cu(CDC) MOF.[9] Further isomer enrichment was achieved even at a 99% initial *m*-xylene concentration as 99.4 ± 0.2% *m*-xylene was measured in the host crystals.

Figure 4B shows separation experiments for the intermediate sized *m*-X and the smaller *p*-X. Again, the average percentage of *p*-X adsorbed by host **1** is plotted against the percentage of *p*-X from the prepared solution and shows that the smaller isomer is selectively absorbed by host **1**. However, lower concentrations of the *p*-X (1.00% and 20.0% *p*-xylene) did have a larger standard deviation across the three trials of selective loading experiments. The deviations in the measurements decreased for the higher *p*-xylene concentrations tested. The 50.0% *p*-xylene solution led to an average loading of 69.4 ± 8.3% *p*-xylene inside the host giving a para/meta selectivity value of 2.2 which is comparable to that of a BaX zeolite between temperatures of 323 to 343 K.[9] No further enrichment was observed from the 99.0% *p*-xylene mixture as an average of 99.0 ± 0.5% *p*-xylene was measured inside the crystalline host.

For the *p*-X versus *o*-X separation, the average percentage of *p*-X is plotted against the percentage of *p*-X from the prepared solution (Figure 4C). Again, selectivity is observed for the absorption of the smaller *p*-X isomer. Comparison of the binary 50:50 isomeric mixtures gave an average loading of 70.7 ± 6.4% inside host **1**. This gives a para/ortho selectivity value of 2.4 which is comparable to that of a BaX zeolite at 343 K.[9] Enrichment of the 99.0% *p*-xylene mixture was observed with 99.5 ± 0.2% *p*-xylene measured inside the host.

Next, competitive vapor loading experiments were performed using a 1:1:1 ternary mixture of xylene isomers. Freshly

https://doi.org/10.1021/acs.cgd.1c00846
Cryst. Growth Des. 2022, 22, 1017−1023

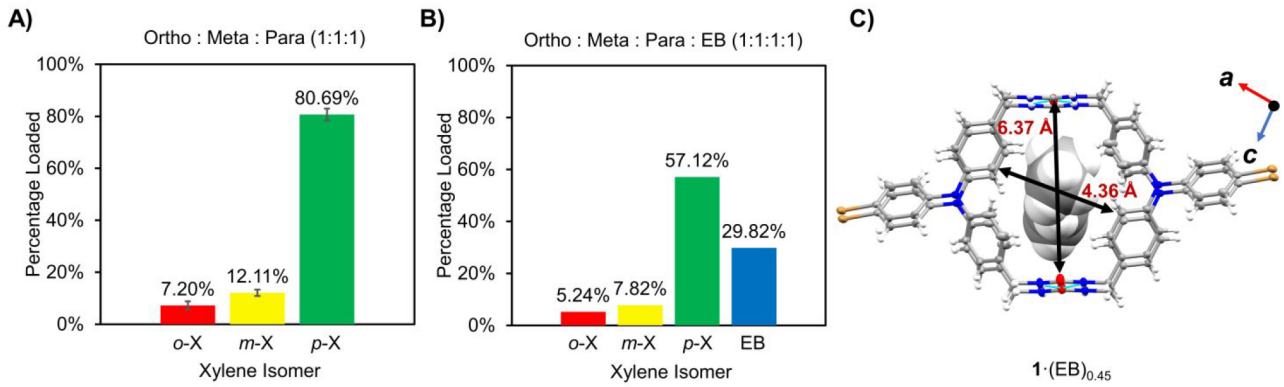

Figure 5. (A) Averaged results from GC/MS data of three trials of selective loading from a 1:1:1 (*o*-X, *m*-X, *p*-X) ternary mixture of xylene isomers. (B) Results from GC/MS data of selective loading from a 1:1:1:1 (*o*-X, *m*-X, *p*-X, ethylbenzene (EB)) quaternary mixture of C8 aromatic compounds. (C) Ethylbenzene loaded $\mathbf{1}\cdot(EB)_{0.45}$ host–guest complex as viewed along the crystallographic *b*-axis.

activated host **1** crystals were exposed to the vapor overnight. Then crystals were removed and suspended in CH_2Cl_2 or CD_2Cl_2 to extract out all the guests, as in prior experiments. The solutions were then examined by GC/MS data, and a control was also evaluated by ^{1}H NMR after direct dissolution in DMSO-d_6. Figure 5A compares the average percent loading values obtained from three separate trials. Again, there is a large difference in selectivity between the three guests with *p*-X preferentially loaded in 80.69% selectivity. In comparison, *m*-X and *o*-X were observed at 12.11% and 7.20% respectively. Overall, the selectivity observed in the ternary competition correlated well with the binary xylene experiments.

Finally, a competitive vapor-loading experiment was conducted on an equimolar mix of the three xylene isomers and ethylbenzene. Here, the host retains a preference for *p*-X (57.12%); however, EB (29.82%) is absorbed over the other xylene isomers. Overall, *m*-X and *o*-X are loaded in lower selectivity 7.82% and 5.24%, respectively, as compared to the ternary mixture. The two favored guests *p*-X and EB have similar smaller kinetic diameters (6.7 Å, Table 1) in comparison to the other isomers (*m*-X 7.1 Å and *o*-X 7.4 Å). While loading selectivity is likely due to complex factors including conformational, supramolecular interactions, packing energy, and other effects, our experiments suggest that kinetic diameter is of key importance in determining selectivity with the narrow channels of host **1**.

CONCLUSIONS

We have demonstrated that host **1** is robust, reusable, and readily absorbs xylene isomers and ethylbenzene in solid–vapor processes. Once the guest is absorbed within the host, it can be removed simply by soaking the crystals in CH_2Cl_2. Guest uptake is reversible and does not appear to impact the quality of the single crystals as these studies employed the same batch of host crystals. Although the crystalline host absorbs each of these compounds separately, when equilibrated with binary or ternary mixtures of xylenes the host shows large differences in selectivity. The selectivity of guest loading was retained throughout the single component studies and 54 selective xylene guest loading experiments.

Single crystal data reveals the pores of host **1** to be adaptive as slight differences in TPA–TPA and urea–urea distances as well as overall void space volume (Figure 2) are observed when comparing each **1**·X complex to the activated host. Although complicated by the existing disorder of the guests, the smaller kinetic diameter isomers (*p*-X < *m*-X < *o*-X)[29] showed less disorder (Figures S3–S6) and exhibited slightly more favorable offset values for π–π interactions for the respective complexes ($\mathbf{1}\cdot(p\text{-X})_{0.5}$ > $\mathbf{1}\cdot(m\text{-X})_{0.5}$ > $\mathbf{1}\cdot(o\text{-X})_{0.5}$, Figure 3B). Further mapping of solvent vapor-induced structural transitions using Hirshfeld surface analysis and full interaction Map calculations has been examined for metal–organic frameworks.[37] We are planning similar analysis on these structures to further probe the origin of this selectivity. Experimentally, higher temperatures were required to remove the smaller $\mathbf{1}\cdot(p\text{-X})_{0.5}$ as observed via TGA, suggesting it forms the most stable complex. However, the observed preferential loading of the smaller isomer in all competitive adsorption studies using ternary and binary mixtures (*p*-X > *m*-X > *o*-X) appears to be driven more by kinetics than thermodynamics. A direct correlation is observed between the kinetic diameter of the guest and preferential loading.

In equimolar mixtures of the three xylene isomers and EB, the host retained selectivity for *p*-X (57.12%) but also showed significant uptake of EB (29.82%). This result again highlighted the importance of kinetic diameters in determining selectivity, as these two guests exhibit similar diameters. Here, the preference for loading *p*-X over EB may be derived from the lower dipole moment of *p*-X or its more linear shape. Isomer loading preferences of host **1** are comparable to other porous adsorbents when loading is accomplished at similar temperatures and without the use of additional solvents.[9] It is advantageous that xylenes can be readily recovered and separated from the host simply by soaking in CH_2Cl_2. Filtration or centrifugation followed by decanting off the solution afforded crystals that were reused for further separations. Currently, we are optimizing and scaling the synthesis of **1** using a dynamic covalent method. We plan to evaluate the efficiency of the host for the separation of *p*-X on a larger scale and in solid–liquid processes. Future work includes the separation of stereoisomers using host **1** for guest molecules with bulky diastereomers and the production of a chiral macrocyclic host for the enrichment of enantiomeric mixtures.

ASSOCIATED CONTENT

Supporting Information

The Supporting Information is available free of charge at https://pubs.acs.org/doi/10.1021/acs.cgd.1c00846.

https://doi.org/10.1021/acs.cgd.1c00846
Cryst. Growth Des. 2022, 22, 1017–1023

Product characterization, NMR, X-ray, TGA, and mass spectrometry (PDF)

Accession Codes

CCDC 2097957−2097960 and 2121650 contain the supplementary crystallographic data for this paper. These data can be obtained free of charge via www.ccdc.cam.ac.uk/data_request/cif, or by emailing data_request@ccdc.cam.ac.uk, or by contacting The Cambridge Crystallographic Data Centre, 12 Union Road, Cambridge CB2 1EZ, UK; fax: +44 1223 336033.

AUTHOR INFORMATION

Corresponding Author

Linda S. Shimizu − *Department of Chemistry and Biochemistry, University of South Carolina, Columbia, South Carolina 29208, United States;* orcid.org/0000-0001-5599-4960; Email: shimizls@mailbox.sc.edu

Authors

Dustin W. Goodlett − *Department of Chemistry and Biochemistry, University of South Carolina, Columbia, South Carolina 29208, United States;* orcid.org/0000-0003-4063-3745

Ammon J. Sindt − *Department of Chemistry and Biochemistry, University of South Carolina, Columbia, South Carolina 29208, United States*

Md Faizul Islam − *Department of Chemistry and Biochemistry, University of South Carolina, Columbia, South Carolina 29208, United States*

Mark D. Smith − *Department of Chemistry and Biochemistry, University of South Carolina, Columbia, South Carolina 29208, United States*

Complete contact information is available at: https://pubs.acs.org/10.1021/acs.cgd.1c00846

Notes

The authors declare no competing financial interest.

ACKNOWLEDGMENTS

This work was supported in part by the National Science Foundation CHE-1904386 and OIA-1655740.

REFERENCES

(1) Ramamurthy, V.; Sivaguru, J. Supramolecular Photochemistry as a Potential Synthetic Tool: Photocycloaddition. *Chem. Rev.* **2016**, *116* (17), 9914−9993.

(2) Dawn, S.; Salpage, S. R.; Koscher, B. A.; Bick, A.; Wibowo, A. C.; Pellechia, P. J.; Shimizu, L. S. Applications of a Bis-Urea Phenylethynylene Self-Assembled Nanoreactor for [2 + 2] Photodimerizations. *J. Phys. Chem. A* **2014**, *118* (45), 10563−10574.

(3) Das, S.; Heasman, P.; Ben, T.; Qiu, S. Porous Organic Materials: Strategic Design and Structure-Function Correlation. *Chemical Reviews* **2017**, *8*, 1515−1563, DOI: 10.1021/acs.chemrev.6b00439.

(4) Dolgopolova, E. A.; Rice, A. M.; Martin, C. R.; Shustova, N. B. Photochemistry and Photophysics of MOFs: Steps towards MOF-Based Sensing Enhancements. *Chemical Society Reviews* **2018**, *7*, 4710−4728, DOI: 10.1039/c7cs00861a.

(5) Evans, J. D.; Huang, D. M.; Hill, M. R.; Sumby, C. J.; Thornton, A. W.; Doonan, C. J. Feasibility of Mixed Matrix Membrane Gas Separations Employing Porous Organic Cages. *J. Phys. Chem. C* **2014**, *118* (3), 1523−1529.

(6) Wang, H.; Li, B.; Wu, H.; Hu, T. L.; Yao, Z.; Zhou, W.; Xiang, S.; Chen, B. A Flexible Microporous Hydrogen-Bonded Organic Framework for Gas Sorption and Separation. *J. Am. Chem. Soc.* **2015**, *137* (31), 9963−9970.

(7) Yang, Y.; Li, L.; Lin, R.-B.; Ye, Y.; Yao, Z.; Yang, L.; Xiang, F.; Chen, S.; Zhang, Z.; Xiang, S.; Chen, B. Ethylene/Ethane Separation in a Stable Hydrogen-Bonded Organic Framework through a Gating Mechanism. *Nat. Chem.* **2021**, *13*, 933−939.

(8) Wang, J.-X.; Gu, X.-W.; Lin, Y.-X.; Li, B.; Qian, G. A Novel Hydrogen-Bonded Organic Framework with Highly Permanent Porosity for Boosting Ethane/Ethylene Separation. *ACS Mater. Lett.* **2021**, *3* (5), 497−503.

(9) Yang, Y.; Bai, P.; Guo, X. Separation of Xylene Isomers: A Review of Recent Advances in Materials. *Ind. Eng. Chem. Res.* **2017**, *20*, 14725−14753, DOI: 10.1021/acs.iecr.7b03127.

(10) Krishna, R. Separating Mixtures by Exploiting Molecular Packing Effects in Microporous Materials. *Phys. Chem. Chem. Phys.* **2015**, *7*, 39−59, DOI: 10.1039/c4cp03939d.

(11) Ambrose, D. Vapour Pressures of Some Aromatic Hydrocarbons. *J. Chem. Thermodyn.* **1987**, *19*, 1007−1008.

(12) Vermeiren, W.; Gilson, J. P. Impact of Zeolites on the Petroleum and Petrochemical Industry. *Top. Catal.* **2009**, *52* (9), 1131−1161.

(13) Li, Y.; Li, L.; Yu, J. Applications of Zeolites in Sustainable Chemistry. *Chem. Elsevier Inc December* **2017**, *3*, 928−949.

(14) Wu, Q.; Wang, X.; Qi, G.; Guo, Q.; Pan, S.; Meng, X.; Xu, J.; Deng, F.; Fan, F.; Feng, Z.; Li, C.; Maurer, S.; Müller, U.; Xiao, F. S. Sustainable Synthesis of Zeolites without Addition of Both Organotemplates and Solvents. *J. Am. Chem. Soc.* **2014**, *136* (10), 4019−4025.

(15) Wang, C.; Guan, E.; Wang, L.; Chu, X.; Wu, Z.; Zhang, J.; Yang, Z.; Jiang, Y.; Zhang, L.; Meng, X.; Gates, B. C.; Xiao, F. S. Product Selectivity Controlled by Nanoporous Environments in Zeolite Crystals Enveloping Rhodium Nanoparticle Catalysts for CO2 Hydrogenation. *J. Am. Chem. Soc.* **2019**, *141* (21), 8482−8488.

(16) Chen, D.-M.; Zhang, N.-N.; Tian, J.-Y.; Liu, C.-S.; Du, M. Pore Modulation of Metal-Organic Frameworks towards Enhanced Hydrothermal Stability and Acetylene Uptake via Incorporation of Different Functional Brackets. *J. Mater. Chem. A* **2017**, *5* (10), 4861−4867.

(17) Fan, W.; Wang, X.; Zhang, X.; Liu, X.; Wang, Y.; Kang, Z.; Dai, F.; Xu, B.; Wang, R.; Sun, D. Fine-Tuning the Pore Environment of the Microporous Cu-MOF for High Propylene Storage and Efficient Separation of Light Hydrocarbons. *ACS Cent. Sci.* **2019**, *5* (7), 1261−1268.

(18) Lin, R. B.; He, Y.; Li, P.; Wang, H.; Zhou, W.; Chen, B. Multifunctional Porous Hydrogen-Bonded Organic Framework Materials. *Chemical Society Reviews* **2019**, *7*, 1362−1389, DOI: 10.1039/c8cs00155c.

(19) Geer, M. F.; Walla, M. D.; Solntsev, K. M.; Strassert, C. A.; Shimizu, L. S. Self-Assembled Benzophenone Bis-Urea Macrocycles Facilitate Selective Oxidations by Singlet Oxygen. *J. Org. Chem.* **2013**, *78* (11), 5568−5578.

(20) Kałuża, A. M.; Mukherjee, S.; Wang, S.-Q.; O'Hearn, D. J.; Zaworotko, M. J. [Cu(4-Phenylpyridine)4-(Trifluoromethanesulfonate)2], a Werner Complex That Exhibits High Selectivity for o-Xylene. *Chem. Commun.* **2020**, *56* (13), 1940−1943.

(21) Kumar, N.; Wang, S.-Q.; Mukherjee, S.; Bezrukov, A. A.; Patyk-Kaźmierczak, E.; O'Nolan, D.; Kumar, A.; Yu, M.-H.; Chang, Z.; Bu, X.-H.; Zaworotko, M. J. Crystal Engineering of a Rectangular Sql Coordination Network to Enable Xylenes Selectivity over Ethylbenzene. *Chem. Sci.* **2020**, *11* (26), 6889−6895.

(22) Mukherjee, S.; Joarder, B.; Manna, B.; Desai, A. V.; Chaudhari, A. K.; Ghosh, S. K. Framework-Flexibility Driven Selective Sorption of p-Xylene over Other Isomers by a Dynamic Metal-Organic Framework. *Sci. Rep.* **2015**, *4* (1), 1−7.

(23) du Plessis, M.; Nikolayenko, V. I.; Barbour, L. J. Record-Setting Selectivity for p-Xylene by an Intrinsically Porous Zero-Dimensional Metallocycle. *J. Am. Chem. Soc.* **2020**, *142* (10), 4529−4533.

(24) Jie, K.; Liu, M.; Zhou, Y.; Little, M. A.; Pulido, A.; Chong, S. Y.; Stephenson, A.; Hughes, A. R.; Sakakibara, F.; Ogoshi, T.; Blanc, F.; Day, G. M.; Huang, F.; Cooper, A. I. Near-Ideal Xylene Selectivity in

Adaptive Molecular Pillar[n]Arene Crystals. *J. Am. Chem. Soc.* **2018**, *140* (22), 6921−6930.
(25) Lusi, M.; Barbour, L. J. Solid−Vapor Sorption of Xylenes: Prioritized Selectivity as a Means of Separating All Three Isomers Using a Single Substrate. *Angew. Chem., Int. Ed.* **2012**, *51* (16), 3928−3931.
(26) Wang, S.-Q.; Mukherjee, S.; Patyk-Kaźmierczak, E.; Darwish, S.; Bajpai, A.; Yang, Q.-Y.; Zaworotko, M. J. Highly Selective, High-Capacity Separation of o-Xylene from C8 Aromatics by a Switching Adsorbent Layered Material. *Angew. Chem., Int. Ed.* **2019**, *58* (20), 6630−6634.
(27) Pivovar, A. M.; Holman, K. T.; Ward, M. D. Shape-Selective Separation of Molecular Isomers with Tunable Hydrogen-Bonded Host Frameworks. *Chem. Mater.* **2001**, *13* (9), 3018−3031.
(28) Lannoeye, J.; Van De Voorde, B.; Bozbiyik, B.; Reinsch, H.; Denayer, J.; De Vos, D. An Aliphatic Copper Metal-Organic Framework as Versatile Shape Selective Adsorbent in Liquid Phase Separations. *Microporous Mesoporous Mater.* **2016**, *226*, 292−298.
(29) Bárcia, P. S.; Guimarães, D.; Mendes, P. A. P.; Silva, J. A. C.; Guillerm, V.; Chevreau, H.; Serre, C.; Rodrigues, A. E. Reverse Shape Selectivity in the Adsorption of Hexane and Xylene Isomers in MOF UiO-66. *Microporous Mesoporous Mater.* **2011**, *139* (1−3), 67−73.
(30) Gonzalez, M. I.; Kapelewski, M. T.; Bloch, E. D.; Milner, P. J.; Reed, D. A.; Hudson, M. R.; Mason, J. A.; Barin, G.; Brown, C. M.; Long, J. R. Separation of Xylene Isomers through Multiple Metal Site Interactions in Metal−Organic Frameworks. *J. Am. Chem. Soc.* **2018**, *140* (9), 3412−3422.
(31) Shimizu, L. S.; Hughes, A. D.; Smith, M. D.; Samuel, S. A.; Ciurtin-Smith, D. Assembled Columnar Structures from Bis-Urea Macrocycles. *Supramol. Chem.* **2005**, *17* (1−2), 27−30.
(32) Salpage, S. R.; Xu, Y.; Som, B.; Sindt, A. J.; Smith, M. D.; Shimizu, L. S. Pyridyl-Phenylethynylene: Bis -Urea Macrocycles: Self-Assembly and Utility as a Nanoreactor for the Selective Photoreaction of Isoprene. *RSC Adv.* **2016**, *6* (100), 98350−98355.
(33) Custelcean, R. Crystal Engineering with Urea and Thiourea Hydrogen-Bonding Groups. *Chem. Commun.* **2008**, 295−307.
(34) Sindt, A. J.; Smith, M. D.; Berens, S.; Vasenkov, S.; Bowers, C. R.; Shimizu, L. S. Single-Crystal-to-Single-Crystal Guest Exchange in Columnar Assembled Brominated Triphenylamine Bis-Urea Macrocycles. *Chem. Commun.* **2019**, *55*, 5619−5622.
(35) Macrae, C. F.; Sovago, I.; Cottrell, S. J.; Galek, P. T. A.; McCabe, P.; Pidcock, E.; Platings, M.; Shields, G. P.; Stevens, J. S.; Towler, M.; Wood, P. A. Mercury 4.0: from visualization to analysis, design and prediction. *J. Appl. Crystallogr.* **2020**, *53*, 226−235.
(36) Banerjee, A.; Saha, A.; Saha, B. K. Understanding the Behavior of $\pi-\pi$ Interactions in Crystal Structures in Light of Geometry Corrected Statistical Analysis: Similarities and Differences with the Theoretical Models. *Cryst. Growth Des.* **2019**, *19*, 2245−2252.
(37) Mukherjee, S.; Sensharma, D.; Qazvini, O.; Dutta, S.; Macreadie, L.; Ghosh, S.; Babarao, R. Advances in adsorptive separation of benzene and cyclohexane by metal-organic framework adsorbents. *Coord. Chem. Rev.* **2021**, *437*, 213852.

https://doi.org/10.1021/acs.cgd.1c00846
Cryst. Growth Des. 2022, 22, 1017−1023